WATER RESOURCES RESEARCH, VOL. 34, NO. 12, PAGES 3349–3367, DECEMBER 1998

# Laboratory experiments on heat-driven two-phase flows in natural and artificial rock fractures

Timothy J. Kneafsey and Karsten Pruess

Earth Sciences Division, Lawrence Berkeley National Laboratory, University of California, Berkeley

**Abstract.** Water flow in partially saturated fractures under thermal drive may lead to fast flow along preferential localized pathways and heat pipe conditions. At the potential high-level nuclear waste repository at Yucca Mountain, water flowing in fast pathways may ultimately contact waste packages and transport radionuclides to the accessible environment. Sixteen experiments were conducted to visualize heat-driven liquid flow in fracture models that included (1) assemblies of roughened glass plates, (2) epoxy replicas of rock fractures, and (3) a fractured specimen of Topopah Spring tuff. Continuous rivulet flow was observed for high liquid flow rates, intermittent rivulet flow and drop flow for intermediate flow rates, and film flow for lower flow rates and wide apertures. Heat pipe conditions (vapor-liquid counterflow with phase change) were identified in five of the seven experiments in which spatially resolved thermal monitoring was performed but not when vapor-liquid counterflow was hindered by very narrow apertures and when an inadequate working fluid volume was used.

## 1. Introduction

Heat released from high-level nuclear waste packages in a partially saturated environment can have major impacts on moisture distribution and migration. The tuff formations in the unsaturated zone at Yucca Mountain contain up to 80% or more liquid water in the pore space [*Pruess et al*., 1990a], which will be vaporized as formation temperatures approach and exceed the boiling point at prevailing pressures. This will cause pressurization of the gas phase which will drive vapor away from the heat source [*Buscheck and Nitao*, 1994]. In a fractured medium the vapor is expected to flow primarily in the fractures. Condensation will take place as the vapor invades cooler rock, which will generate mobile water in the fractures which will flow under the combined action of gravity and capillary forces. In addition to imbibition into the rock matrix, it may, in part, return to the vicinity of the waste packages where it would again be subject to vaporization [*Buscheck and Nitao*, 1993]. Mathematical modeling studies have indicated that vaporization may not be complete. Water flowing down (sub-) vertical fractures may partially escape vaporization and may migrate considerable distances through fractured rock that is at above boiling temperatures [*Pruess*, 1997]. This raises the concern that flowing condensate may contact waste packages and provide a pathway for the transport of water-soluble radionuclides.

The amount of water that could be generated by vaporization-condensation cycles is potentially very large. A single multipurpose canister can generate condensate at an average rate of several cubic meters per year over a 10,000 year period. For a nominal thermal loading of 57 kW acre$^{-1}$ this translates into an average equivalent percolation flux from condensate of 23.1 mm yr$^{-1}$ over 1000 years and 5.2 mm yr$^{-1}$ over 10,000 years [*Pruess and Tsang*, 1994]. These numbers are comparable to or larger than current estimates of net infiltration at Yucca Mountain [*Flint et al*., 1996]. The condensate would be generated in the immediate vicinity (meters) of the waste packages, so its impact on waste package and repository performance is likely to be larger than the impact of a similar amount of water introduced at the land surface.

These considerations suggest that thermally driven flow processes induced by repository heat may well be as important or even more important for repository performance than natural infiltration [*Buscheck and Nitao*, 1993; *Pruess and Tsang*, 1994]. A combined program of field, laboratory, and theoretical studies is needed to gain an understanding of these processes so that they may be properly taken into account for waste package and repository design and for repository performance evaluation. Key issues include the extent of formation dry-out and liquid-phase exclusion from regions heated above the nominal boiling point, the formation and behavior of condensation zones, the potential development of fast preferential water flow paths, the migration of transient water pulses through heated regions, and the development of heat pipe conditions. There is a long track record of mathematical modeling studies devoted to thermally driven processes in the Yucca Mountain Project [*Nitao*, 1989; *Nitao et al*., 1992; *Pruess and Tsang*, 1993, 1994; *Pruess et al*., 1984, 1988, 1985, 1990a, b; *Tsang and Pruess*, 1987, 1989]. Additionally, there have been many theoretical and experimental studies of the behavior of heat pipes primarily in porous media [*McGuinness*, 1996, 1997; *Ramesh and Torrance*, 1990; *Stubos et al*., 1993; *Udell*, 1985]. Most of these studies have used modeling approaches that involved some form of volume averaging and homogenization of heterogeneous formation properties. Laboratory and field experiments on thermally driven flow processes are needed to provide guidance for the modeling work. Field-scale tests such as the single-heater test and the drift-scale test have been or will be performed at Yucca Mountain [*Birkholzer and Tsang*, 1996, 1997].

Laboratory investigations examining flow in fracture replicas and models under isothermal conditions have provided insights into wetting front instabilities, finger formation, and thread snapping under various liquid loading rates, relative gravita-



Paper number 98WR02035.
0043-1397/98/98WR-02035$09.00

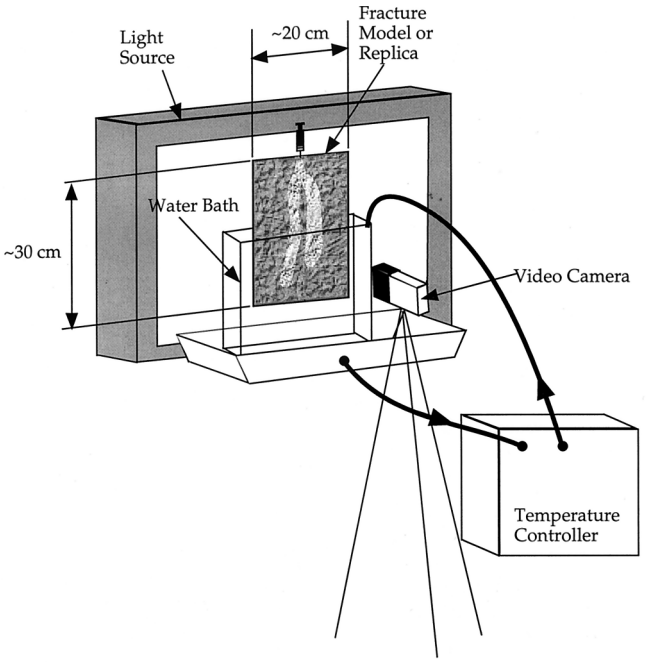


**Figure 1.** Experimental setup. The transparent fracture model is set in front of the light source. Light is more directly transmitted (appears brighter) where the fracture walls are wet and most directly transmitted where the aperture is saturated with liquid.

tional forces, and two-phase relative permeability [*Geller et al*., 1996; *Glass and Nicholl*, 1995; *Glass and Norton*, 1992; *Nicholl et al*., 1992, 1993a, b; *Persoff and Pruess*, 1995]. Nonisothermal investigations of liquid flow in two-dimensional porous media have been performed providing liquid and gas flow information [*Ho et al*., 1994]. In an investigation of recharge of geothermal reservoirs a volatile liquid was introduced into a hot or layered hot and cold sand pack. Heat transfer by evaporation and condensation and unstable fingering were observed in these experiments [*Fitzgerald et al*., 1996].

We present and discuss results of a number of laboratory experiments we performed to visualize and study thermally driven liquid flow phenomena in fracture models, including preferential liquid flow paths in fractures and the development of heat pipes. Experiments have been performed to investigate the thermally driven movement of liquid in a partially saturated fracture at elevated temperatures and examine the likelihood that heat pipe conditions can develop in fractures. The focus of the present paper is a qualitative exploration and discussion of coupled two-phase flow and heat transfer phenomena. Quantitative analysis and issues of scale-up to field conditions will be discussed in a separate paper (in preparation).

## 2. Flow Visualization Experiments

Sixteen experiments were performed in fracture models and fracture replicas. The fracture model and replica surface faces were selected to provide a range of possible fracture surface roughnesses and topographies. Fracture models were composed of various assemblies of sandblasted obscure (textured) and flat glass plates. Transparent epoxy fracture replicas were cast in silicone molds taken from natural fracture faces. Flow experiments were conducted in which some regions of the fracture models and replicas were subjected to temperatures exceeding the boiling point of the liquid, while other regions were maintained below the boiling point. A typical experimental setup is shown in Figure 1.

Glass fracture models were prepared using ordinary 1/4 inch thick flat plate glass and 3/16 inch thick P516 obscure glass (Berkeley Glass Center, Berkeley, California). The obscure glass has a random pattern of rounded projections and depressions, with an estimated amplitude of the order of 100 $\mu$m, and a projection-to-projection spacing of ~2 mm. Sandblasting was used to roughen many of the glass plates, resulting in small pits covering the entire surface. Two sizes of aluminum oxide grit (80 and 240) were used on different pieces of glass to impart different roughnesses. The 80 grit left pits estimated to be of the order of 10 $\mu$m deep. The 240 grit left smaller pits, resulting in a smoother surface. Large sheets of flat glass may vary from being truly flat by up to 150 $\mu$m; however, the glass plates used in these experiments appeared to be flat. Prior to assembly into fracture models the glass plates were washed in a tap water and Liquinox® solution, rinsed well in tap water, rinsed again in distilled water, and allowed to soak for ~1 hour in distilled water prior to air drying. Fracture models were assembled by clamping together clean plates of glass sized 21.6 × 33 cm with or without shims and applying epoxy to the bottom, side, and top edges, leaving three approximately evenly spaced 1.5 cm openings on the top.

Transparent fracture replicas are epoxy casts (Eccobond 27, W.R. Grace Co., Canton, Massachusetts) made from a silicone mold (Silpak R2230, Silpak Inc., Pomona, California) of the fracture surfaces. Both the silicone mold and the epoxy cast are cured at room temperature. Details of the replica-making procedure, originally developed by *Gentier* [1986], are described by *Su* [1995] and *Persoff and Pruess* [1995].

Pentane was used instead of water as the working fluid because the lower boiling point (36.1°C at 1 atm pressure) simplifies the experimental setup. This also allows for a more accurate portrayal of expected boundary conditions because the pentane boiling point is closer to the ambient laboratory temperature, thus producing lower temperature gradients more akin to what would be expected in heating geologic media. Pentane wets the air-glass, air-rock, and air-epoxy interface as water is generally assumed to wet air-mineral interfaces. Normal-boiling-point properties of interest include viscosity (pentane $2.02 \times 10^{-4}$ Pa s [*Vargaftik*, 1975] and water $2.84 \times 10^{-4}$ Pa s [*Lide*, 1990]), interfacial tension (pentane $1.42 \times 10^{-2}$ N m$^{-1}$ [*Rossini et al*., 1953] and water $5.89 \times 10^{-2}$ N m$^{-1}$ [*Lide*, 1990]), density (pentane 613.5 kg m$^{-3}$ [*Rossini et al*., 1953] and water 958.4 kg m$^{-3}$ [*Lide*, 1990]), and enthalpy of vaporization (pentane 357.4 kJ kg$^{-1}$ [*Rossini et al*., 1953] and water 2257 kJ kg$^{-1}$ [*Wark*, 1977]). Pentane is more easily boiled in the experiments than water would be, allowing upward scaling. Pentane's lower interfacial tension would cause pentane to drain by gravity more easily in an unsaturated region, although this would be somewhat offset by density differences.

Detailed information regarding the conditions under which the experiments were performed is presented in Table 1. In Table 1 the experiment number is followed by the designations that describe the two fracture model or replica faces. The designations include SOG for sandblasted obscure glass, SFG for sandblasted flat glass, and FG for flat glass. Thus SOG/FG represents a fracture model with one face sandblasted obscure

**Table 1.** Description of Experiment Conditions

| Experiment/Description[a] | Estimated Aperture Distribution | Surface Roughness[b] | Spatial Heat Application | Temporal Heat Application[c] | Infrared Temperature Monitoring | Other |
|---|---|---|---|---|---|---|
| 1 SOG/FG | near zero to an estimated few hundred microns; random pattern of narrow/wide apertures spaced ~1 mm apart | coarse, one face | ···[d] | 33.8 - 41.8 - 34.8 - 39.2 | no | ··· |
| 2 SOG/FG | see experiment 1 | see experiment 1 | ···[d] | 22 - 43.8 | no | pentane entirely contained within warmed region at startup |
| 3 SFG/FG | near zero to an estimated hundred microns with pattern of narrow/wide apertures due to sandblasting spaced ~2 cm apart | coarse, one face | ···[d] | 33.1 - 40.0 - 35.0 | no | ··· |
| 4 SOG/SOG | near zero to several hundred microns with random pattern of narrow/wide apertures spaced ~1 mm apart (more variable than SOG/FG) | coarse, both faces | ···[d] | 33.8 - 43.8 - 34.8 | no | ··· |
| 5 SOG/SOG | see experiment 4 | see experiment 4 | ···[d] | 33.6 - 41.2 - 23.2 | no | two infiltration events |
| 6 SFG/SFG | near zero to an estimated few hundred microns with a vertical pattern of narrow/wide apertures spaced ~2 cm apart (more variable than SFG/FG) | coarse, both faces | ···[d] | 31.4 - 42.2 - 22.2 | no | ··· |
| 7 SOG/SOG circular heated regions | see experiment 4 | see experiment 4 | circular warmed disks attached to model | 50.6 - 32.2 | no | ··· |
| 8 SOG/FG finger location repeatability | see experiment 1 | see experiment 1 | ···[d] | 37.0 - 38.8 | no | fracture sequentially submerged and raised to observe location of finger formation |
| 9 SFG/SFG wall thickness/heat pipe development | see experiment 6 | see experiment 6 | ···[d] | 36.5 - 42.4 - 34.6 (thin), 37.2 - 42.2 - 36.4 (thick) | yes | ··· |
| 10 SFG/SFG nonuniform heating | see experiment 6 | see experiment 6 | ···[d] | 34.6 - 40.8 - 33.0 | no | Lexan strips (1.9 × 2.5 cm) placed across model to alter heat flow |
| 11 SOG/SOG impermeable barriers | see experiment 4; impermeable epoxy barriers placed to form a funnel and focus flow | coarse, both faces | ···[d] | 34.8 - 42.2 - 34.8 | yes | ··· |
| 12 SFG/SFG wide aperture | nominal aperture of 0.76 mm | coarse, both faces | ···[d] | 33.0 - 39.0 - 32.3 | yes | ··· |
| 13 SOG/SOG fine surface roughness | near zero to several hundred microns with random pattern of narrow/wide apertures spaced ~1 mm apart (more variable than SOG/FG) | fine, both faces | ···[d] | 32.4 - 42.1 - 3.8 | yes | open side at top right |
| 14 SFG/SFG fine surface roughness | ~100 $\mu$m or less | fine, both faces | ···[d] | 34.1 - 38.3 - 32.2 | yes | ··· |
| 15 Stripa replica | near zero to 1000 or more microns. Cast epoxy replica of natural fracture in deep granite from Stripa Mine, Sweden | small-scale fairly smooth, intermediate-scale variable | ···[d] | 35.7 - 42.8 | yes | ··· |
| 16 Fran Ridge replica/ rock | near zero to 1000 or more microns; cast epoxy replica of one face of a natural fracture (Topopah Spring tuff from Fran Ridge) mated to the corresponding rock face | large-scale round and smooth, small-scale similar to 80 grit sandblasting on glass | locally heated with heating strips and heat gun | Hot spot cooled from 61.0 - 38.0. | Intermittent, rock face | ··· |

[a]SOG, sandblasted obscure glass; FG, flat glass; and SFG, sandblasted flat glass.
[b]Coarse, 80 grit sandblasting; and fine, 240 grit sandblasting.
[c]Degrees Centigrade.
[d]Model partially submerged in heated bath.

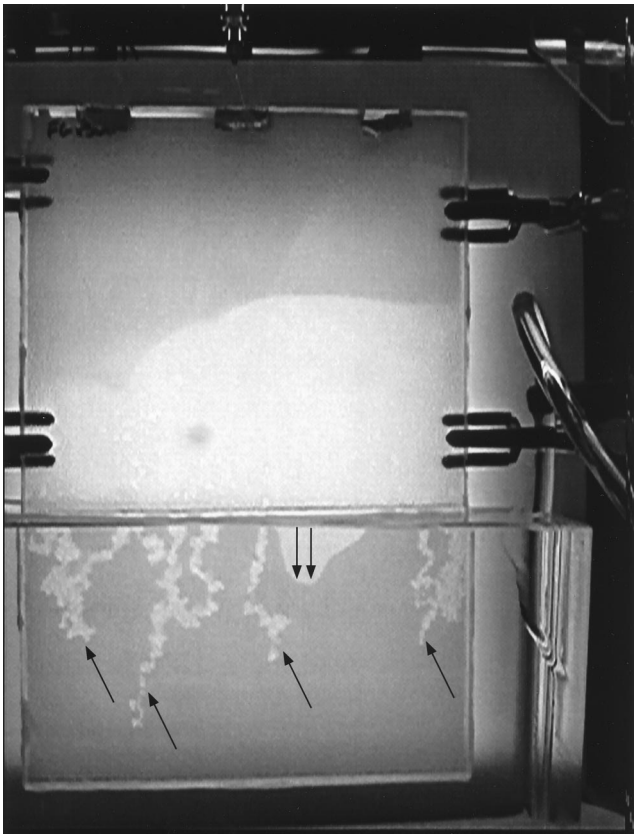

**Figure 2.** Fingers, identified by arrows, and film region (double arrow): experiment 1, 37.2°C $< T_{bath} <$ 37.6°C.

glass and the other face flat glass. Some fracture models were used in several experiments.

The experiments were conducted by applying heat to a portion of the model or replica and introducing pentane into the void space. Temperature changes in experiments occurred on a timescale of 1°C per tens of minutes, whereas liquid injections occurred on a timescale of seconds to minutes. In experiments 1–15 a light source was placed behind the model to allow for direct visualization of the liquid pentane in the fracture (Figure 1). In experiment 16 the replica of one fracture face was mated to the corresponding rock fracture face, and the light source was placed in front of the replica to illuminate the fracture. Experiments were videotaped using a JVC KY-F55BU camera with a JVC HZ-610MDU 6–60 mm motorized zoom lens with a Kenko 2 close-up filter and recorded on a Sony SVHS SVO-5800 video recorder with time coding providing temporal resolution of 1/30 s.

Direct visualization of the liquid behavior in the models and replicas is possible without the addition of dyes because light is more easily transmitted where the surface(s) of the fracture models and replicas is wet, with the brightest regions occurring where the aperture is saturated (spanned) with liquid. Less bright regions occur generally in two brightness levels between the brightness level of the dry roughened glass (darkest, more gray in the black and white images, more red in the color images) and the saturated aperture (brightest, more white in the black and white images, more yellow in the color images). Intermediate brightness levels represent different pentane film thicknesses on multimodal surface roughness, giving a qualitative indication of different liquid saturations. Different brightness levels were also observed when a film was present on only one fracture face. This was distinguishable from different film thicknesses by viewing both sides of the model from an oblique angle during the experiment. In the epoxy replica, brighter regions also occur where films of pentane were present; however, no multiple brightness level differences in films were distinguished.

Spatially resolved temperatures above the warmed region were monitored using an infrared camera (Inframetrics PM 200 Thermacam, SN 8954, 256 × 256 pixels) in seven of the sixteen experiments listed in Table 1. The temperatures recorded by the infrared camera are of the front glass or epoxy surface and are indicative of the temperatures within the aperture but lower because of convective heat loss to the atmosphere. Thermal imaging of the portion of the model submerged in the water has not been performed.

## 3. Observed Flow Behavior

A summary of major observations is presented in Table 2. In experiments 1–6 and 8–15 the fracture models and replicas were partially submerged in a glass tank into which temperature-controlled water was constantly supplied. The temperature of the water bath was set near but below the pentane boiling point at the beginning of the experiment in experiments 1–6 and 10–15 and above the boiling point in experiments 7–9, and the model was allowed to equilibrate with the water (Table 1). After equilibration, pentane was introduced into the fracture model or replica aperture. The pentane seeped downward, influenced by gravity, viscosity, and capillarity. When the pentane flowed into the warmed region either above or below the boiling point, a visible zone of condensation or condensation halo formed in the cooler region above the heated bath. The temperature of the bath was increased over time to above the pentane boiling point to observe the drying out of the warmed region. Dry-out proceeded with liquid pentane in the warmed region evaporating out and condensing in the condensation halo. In the condensation halo the pentane began to travel downward, either in films along the fracture wall or fingering in intermittent or continuously flowing trickles or rivulets that saturate the aperture (Figure 2). As the temperature of the warmed region approached and exceeded the pentane boiling point, pentane gas bubbles (formed by boiling) struggled to escape the bounds of saturated regions. Often this was relatively uneventful; however, rapid evaporation events (REEs) (Figure 3) were frequently observed. In a REE volume of pentane superheats and vaporizes quickly, rapidly expelling droplets of remaining pentane in many directions. In one case (experiment 2) a rather large REE occurred during dry-out, sending a visible cloud of pentane upward at a rate of ~30 cm $s^{-1}$. After dry-out of the warmed region occurred, pentane continued to flow back into the warmed region; however, the depth to which fingers and films penetrated the warmed region decreased as the bath temperature increased.

Experiment 7 was conducted by attaching transparent disks to the fracture model through which water from the temperature controller could flow (Figure 4). The circular warmed regions were heated to ~50°C, well above the pentane boiling point, and pentane was introduced to the top of the system. This setup was designed to model, in an idealized fashion, the (partial) dry-out processes that are expected in fractures intersecting emplacement drifts at Yucca Mountain. As the pentane reached the warmed region of the fracture model surrounding

**Table 2.** Major Observations

| Experiment/Description | Films in WR[a] When Boiling Hot | Fingers in WR | REEs[b] | Heat Pipe | Other |
|---|---|---|---|---|---|
| 1 SOG/FG[c] | yes[d] | yes[d] | yes | ...[e] | ... |
| 2 SOG/FG | yes[d] | yes[d] | yes, large REE during dry-out | ...[e] | ... |
| 3 SFG/FG | no | yes[d] | no | ...[e] | ... |
| 4 SOG/SOG | yes[d] | yes[d] | yes | ...[e] | ... |
| 5 SOG/SOG | yes[d] | yes[d] | yes | ...[e] | longer fingers were present with more pentane |
| 6 SFG/SFG | no | yes[d] | many violent REEs | ...[e] | REEs affected location of saturated islands and film thicknesses in the condensation halo |
| 7 SOG/SOG circular heated regions | no | yes,[d] upon rapid flow | yes | ...[e] | stable, dry region beneath the warmed disks except when large pentane seepage occurred, causing fingers to flow into warmed region |
| 8 SOG/FG finger location repeatability | no | yes | NA | ...[e] | major fingers formed in approximately the same location when submersion depth was the same; however, the same number of fingers did not always form |
| 9 SFG/SFG wall thickness/heat pipe development | yes,[d] thin; no, thick | yes[d] | many violent REEs with thinner glass; Fewer less violent REEs with thicker glass | yes | longer, wider fingers occurring with thicker glass; heat pipe regions of similar size and shape for thin and thick glass |
| 10 SFG/SFG nonuniform heating | no | yes[d] | yes | ...[e] | on warming, Lexan strips hindered heat flow into model in warmed region and impeded heat flow out of model in nonwarmed region; On cooling the lexan hindered heat flow out of the model in both regions; these heat flow heterogeneities altered the condensation halo location, finger location, and length |
| 11 SOG/SOG impermeable barriers | no | yes,[d] longer fingers were present from the funnel center than other locations | ... | yes, outside funnel region | condensation halo and fingers initially formed below barrier; later, pentane pooled in the funnel center, and pentane vapor traveled upward on the outside of the funnel; the number of fingers under the funnel was not constant; gas pressure was higher below the barriers |
| 12 SFG/SFG wide aperture | yes[d] | no, drop flow occurred | no | yes | pentane condensing on the model top resulted in drops which rapidly fell through the model |
| 13 SOG/SOG fine surface roughness | no | yes,[d] finger length longer on right side | no | yes, greater on right side | the size of the condensation halo was somewhat limited by the location of the side vent |
| 14 SFG/SFG fine surface roughness | no | yes,[d] very short | no | no | extremely narrow aperture made introduction of pentane difficult due to capillary and viscous controls; flow-formed saturated islands contained numerous voids, condensation-formed islands were completely filled |
| 15 Stripa replica | yes[d] | yes[d] | yes | yes | rapidly falling drops like in experiment 12, intermittent fingers, and flowing fingers observed |
| 16 Fran Ridge replica/ rock | yes, short-lived | yes, predominant in warmed region | not seen | no | imbibition into the dry rock limited observation time and vapor-liquid counterflow; Heat pipe not observed because of pentane volume, rock size mismatch |

[a]WR, warmed region.
[b]REE, A rapid evaporation event occurs when a volume of liquid suddenly reaches its boiling point and rapidly evaporates on a timescale of tenths of a second, often forcing liquid droplets to move quickly away from the evaporation point.
[c]SOG, sandblasted obscure glass; FG, Flat Glass; and SFG, sandblasted flat glass.
[d]Length decreased with increasing temperature.
[e]No thermal monitoring.

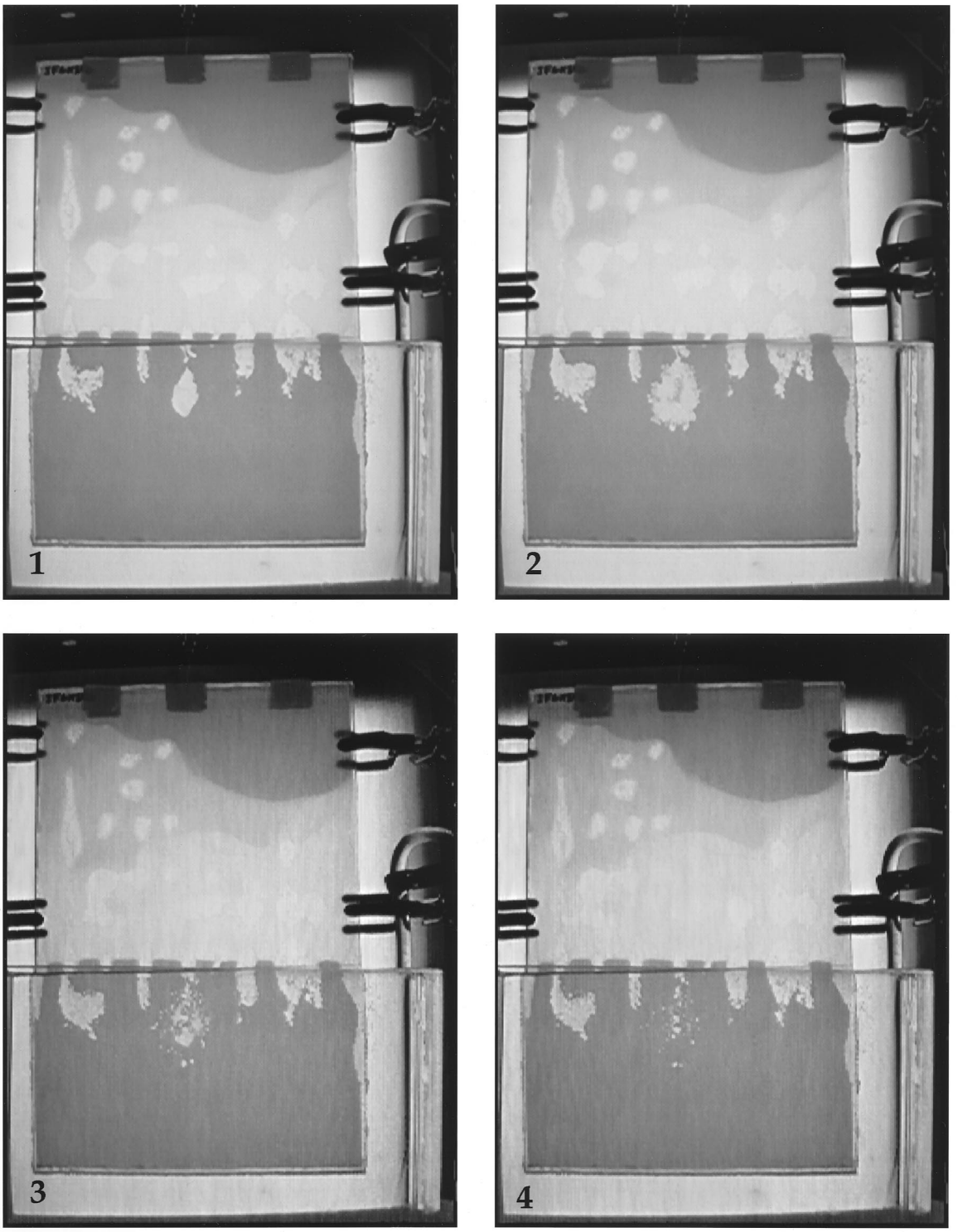


**Figure 3.** Rapid evaporation event in center finger: $t = 0$, 2/15, 6/15, and 1 s.

the heated disks, its apparent further downward motion was impeded. After pentane built up above and finally penetrated the warmed region a condensation halo appeared surrounding the warmed region. When pentane was introduced rapidly, fingers seeped deeply into the warmed region (Figure 4). Between liquid injections, liquid flow occurred primarily by film drainage that did not penetrate deeply into the warmed region. When the warmed region cooled to below the pentane boiling point, pentane films flowed through the warmed region.

Experiment 8 was conducted to determine whether the location of fingers was repeatable when the experimental conditions were similar. The fracture model containing pentane was sequentially lowered to predetermined locations into a constant temperature bath exceeding the pentane boiling point,

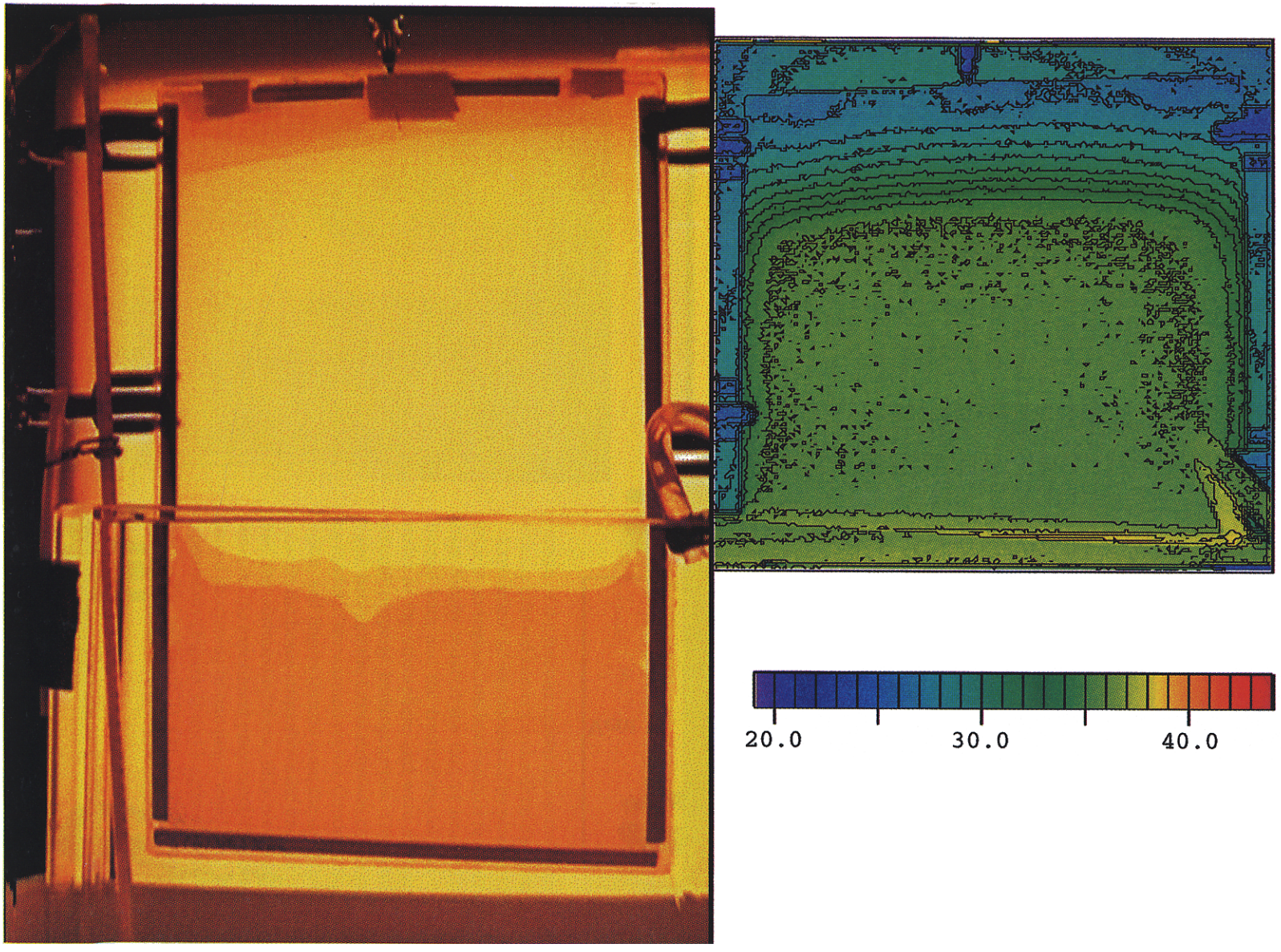


**Plate 1.** (left) Pentane and (right) temperature distributions: experiment 12, 38.6°C $< T_{\text{bath}} <$ 38.8°C. The heat pipe (bright green) region is uniform.

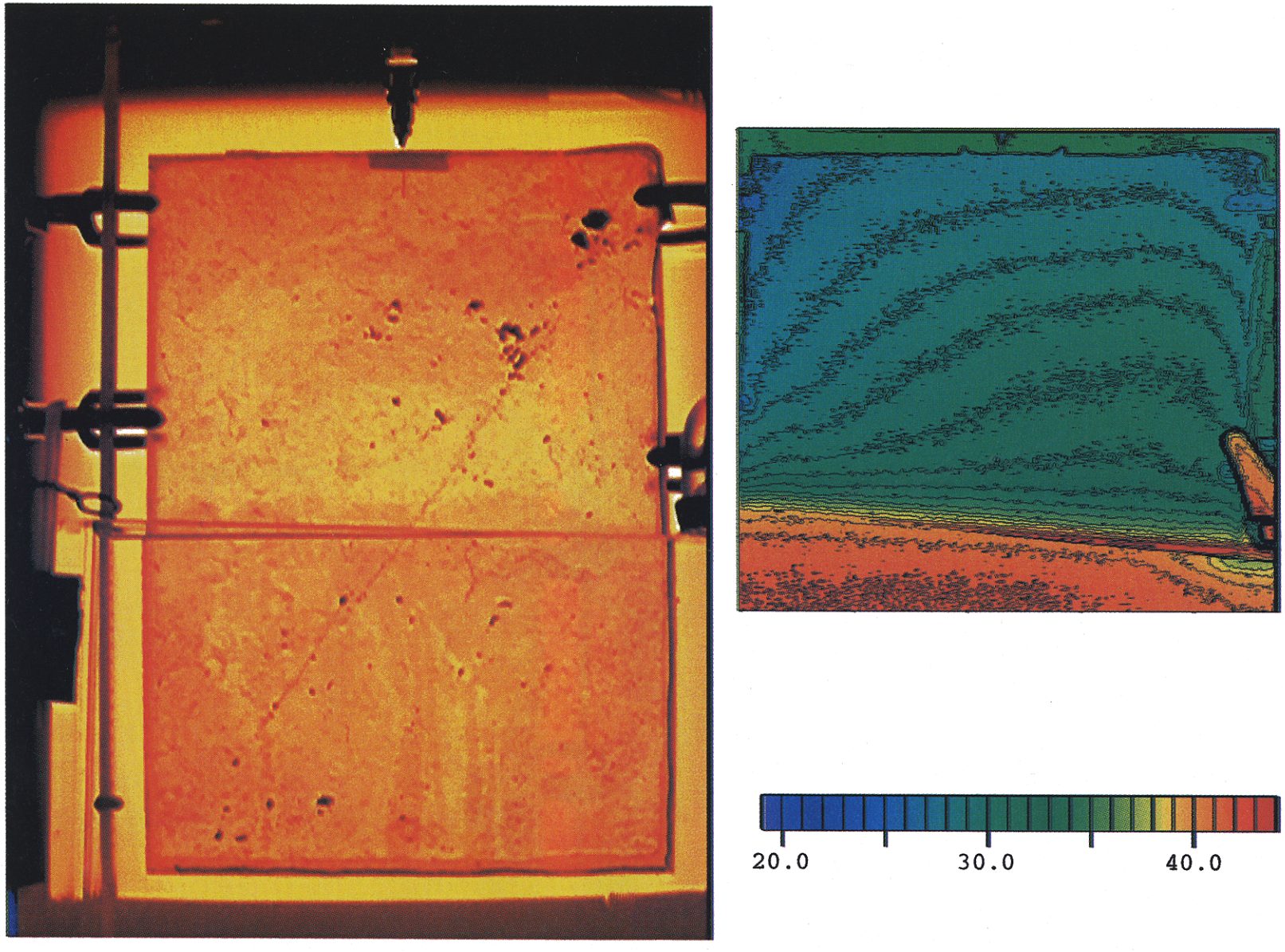


**Plate 2.** (left) Pentane and (right) temperature distributions: experiment 13, 37.2°C $< T_{\text{bath}} <$ 37.8°C. The bright green heat pipe region is more extensive on the right side.

maintaining it at these locations for some time (>10 minutes), and recording the location of the fingers. The model was then sequentially raised to the same locations, again allowing some time at each location (>10 minutes) to observe where fingers formed. Major fingers formed in the same locations when the model was set at a particular height; however, the same number of fingers did not always form. Smaller fingers formed in different locations when the model was set to the same height. This may be because the amount of pentane in the system was not constant throughout the duration of the experiment due to evaporative loss and intermittent replacement.

In Experiment 9 the fracture model was allowed to equilibrate with warmed water exceeding the pentane boiling point prior to the introduction of pentane. Figure 5 shows that although pentane was introduced through the middle port, capillary forces drew the pentane horizontally to the left, after which a pathway downward was encountered. Pentane was not as readily drawn to the right because of aperture heterogeneities. When the pentane penetrated the warmed region, it began to boil, and a condensation halo quickly formed above the warmed region. Fingers of the condensing pentane from this halo then formed in locations that were previously dry. The experiment was repeated with 1/2 inch glass plates added on both sides of the fracture model to reduce the rate of heat transfer from the water bath to the fluid in the fracture. Broader fingers penetrated farther into the warmed region when the heat transfer was reduced (Figure 6). Thicker glass may tend to model more accurately the heat transfer through fractured rock where thick rock matrix of low permeability exists between fractures. Temperature measurements of the portion of the fracture model above the water bath were made with an infrared camera and will be discussed in section 4.

**Figure 5.** Seepage and condensation halo (double arrow) formation; pentane was introduced at the single arrow: experiment 9, $T_{\text{bath}} \sim 36.5$°C.

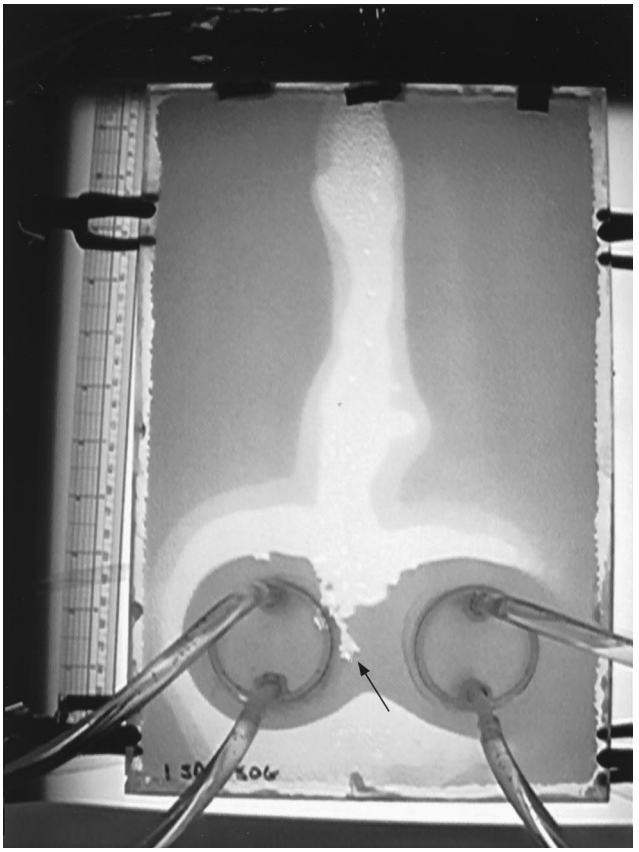

**Figure 4.** Finger (arrow) between and through warmed circular regions (50.6°C): experiment 7.

Experiment 10 was conducted by placing 1.9 × 2.5 cm Lexan strips at an angle across both sides of the fracture model. These strips locally reduced the rate of heat transfer between the thermal bath and the fracture model and from the fracture model to the atmosphere and were intended to model rock thermal property heterogeneities. On heating the bath the region between the Lexan strips was cooler than the surrounding model in the warmed region. Condensation occurred in this region, and fingers formed from the condensation. The region between the Lexan strips above the warmed region was warmer than the surrounding area; thus condensation was reduced there. As the experiment progressed, the heating heterogeneity caused shortening of one finger which had formed in previous experiments (Figure 7) and lengthening of an adjacent finger (not visible in Figure 7). On cooling, the Lexan strips caused the region between the Lexan strips within the warmed region to remain warmer than the surroundings, thus hindering condensation and film flow.

The fracture model used in experiment 11 was constructed using sandblasted (80 grit) obscure glass. Epoxy barriers were placed on one face of the glass at an angle of ~20° from horizontal to form funnel-like structures, and the plates were pressed together and cemented around the edges leaving vents on the top as in previous experiments (Figure 8). Funnel-like structures are of interest because they have been observed in soils [*Kung*, 1990a, b] and are capable of focusing flow into localized preferential paths. Seepage through the model was

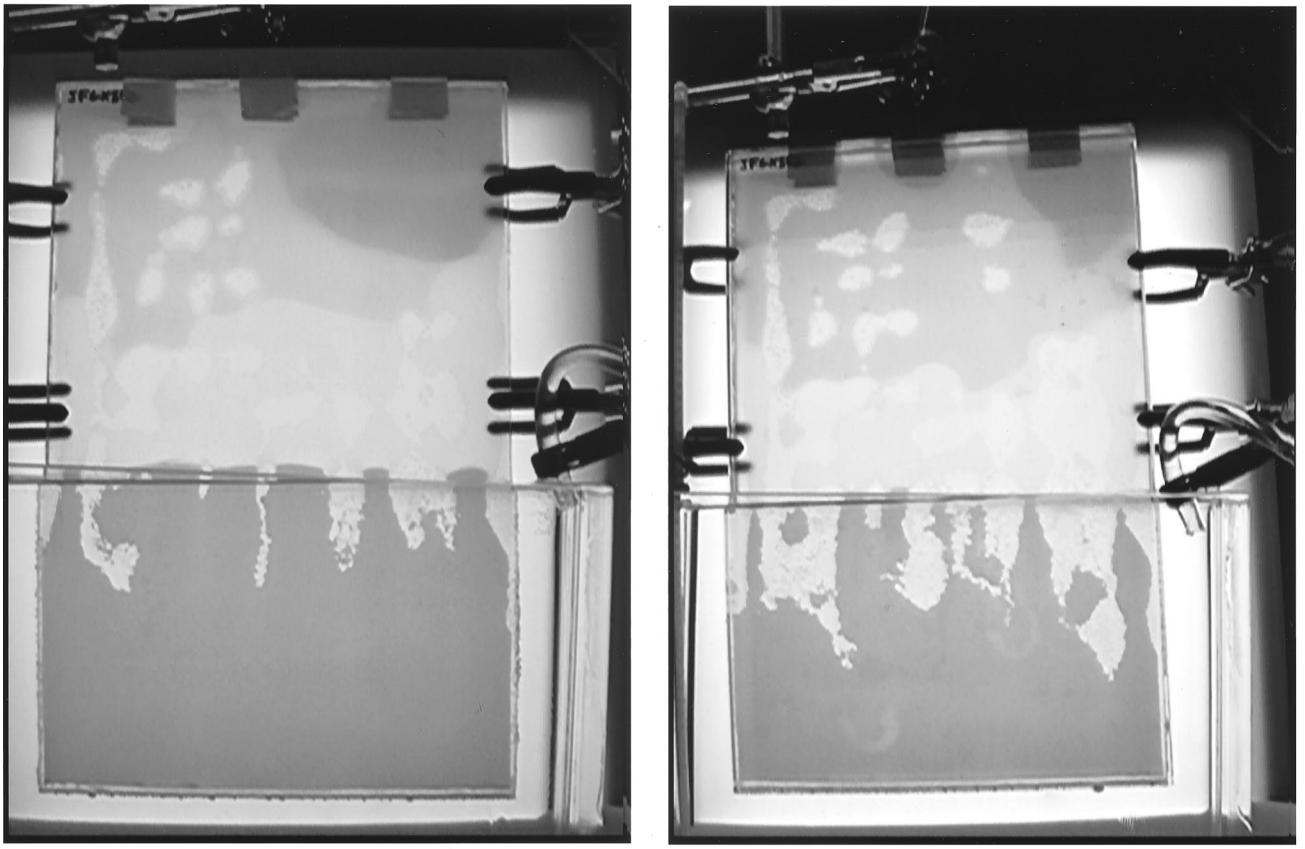

**Figure 6.** Finger length and width. Experiment 9: (left) thin glass and (right) thick glass; $T_{\text{bath}} = 38.8°\text{C}$.

divided by the barriers. Pentane saturated the aperture in the center of the funnel obstructing vertical gas flow there, forcing gas to flow in pathways outside of the funnel structure. When pentane seeped into the warmed region, a condensation halo formed first under the right barrier and later in vertical regions to the left and right of the funnel. Fingers formed from these halos, with short fingers forming under the barrier and longer fingers forming on the left and right of the funnel. The longest fingers flowed from the pathway between the lower barriers (Figure 8). Temperature measurements made of the upper part of the fracture model are discussed in section 4.

The fracture model used in experiment 12 was composed of two sheets of sandblasted (80 grit) flat glass cemented together with three thicknesses of 0.254 mm brass shims around the edges, providing a nominal aperture of 0.76 mm. This models a wide vertical fracture with a few contact points at the boundaries. Upon introduction, pentane flowed straight downward rapidly to the model bottom. The warmed region of the model was near the pentane boiling point, and a condensation halo appeared soon after injection. Because of the wide aperture, pentane was held in films on the fracture faces, and no saturated islands formed. Following the evaporation of all of the pooled pentane in the warmed region, steady films of different lengths on each fracture face were observed flowing downward into the warmed region (Plate 1 (left); Plate 1 (right) will be discussed below). Additional volumes of pentane were added resulting in the condensation halo extending farther both vertically upward and downward. When enough pentane was added so that the films extended to the top of the model, drops of pentane condensed on the shims at the model top and fell downward with speeds of the order of 50 cm $s^{-1}$, slowing in the dry, warmed region, but frequently reaching the model bottom.

Experiment 13 was conducted with a model composed of two sheets of sandblasted (240 grit) obscure glass. A region 12 cm long on the right side, 5.5 cm above the warmed region, was left open. This caused a rapid loss of pentane (compared with other experiments) and tended to keep the height of the condensation halo below the vent. Longer fingers formed on the right side (Plate 2 (left); Plate 2 (right) will be discussed below). This is likely due to pentane vapors being forced under a pressure gradient from their point of evaporation toward the atmospheric pressure boundary at the side vent. Condensation of this vapor would occur as the pentane moved toward the vent, resulting in a net mass flux to the right and the production of longer fingers.

Experiment 14 was conducted with a model composed of two sheets of sandblasted (240 grit) flat glass. This model had the narrowest aperture of all models investigated, and thus viscous flow resistance was the highest, and capillary effects were the strongest. Pentane was very difficult to introduce into the model because of pentane spreading near the top of the model saturating the aperture and plugging the vents. Once introduced, pentane slowly seeped downward through the model. After the boiling temperature of pentane was reached, very short fingers penetrated the warmed region. Saturated islands of pentane were present throughout the upper region. Saturated islands formed by liquid flowing contained many voids because capillary forces caused liquid to flow around locally wider apertures. Condensing vapor filled locally wider

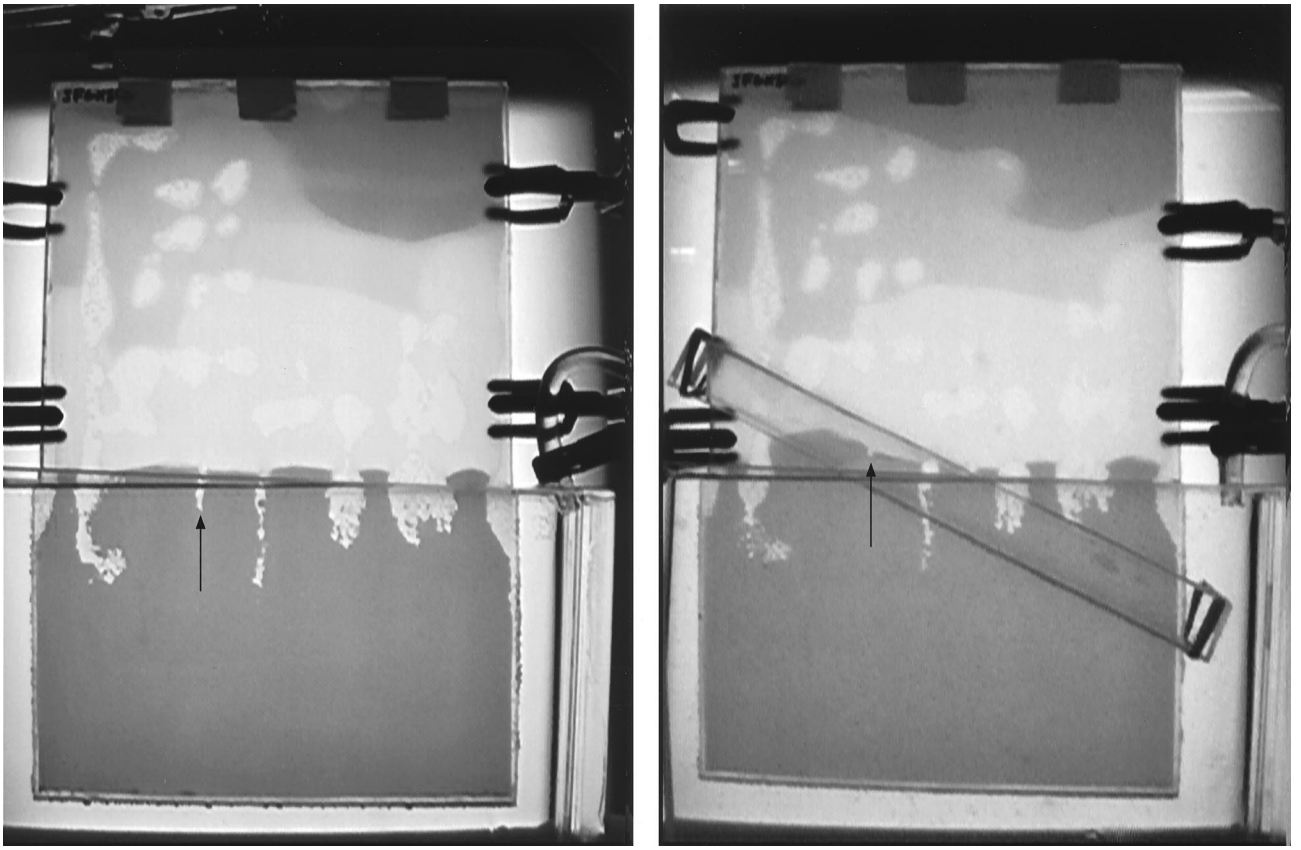

**Figure 7.** Finger length altered by heterogeneous heat transfer: (left) experiment 9 and (right) experiment 10. $T_{bath}$ = 39.6°C and 39.8°C, respectively.

apertures (pits in walls); thus saturated islands formed by condensation did not contain voids.

Experiment 15 was conducted using an epoxy fracture replica with dimensions 21.8 × 30.3 × ~3.7 cm made from both faces of a natural fracture from a granite core obtained from the Stripa mine in Sweden. This replica had yellowed with age, making different levels of brightness difficult to distinguish (Plate 3 (left); Plate 3 (right) will be discussed below). This particular fracture and replicas thereof have also been used in a series of isothermal water flow experiments at ambient temperatures [*Geller et al*., 1996]. The replica faces were mated and sealed together with epoxy like the fracture models, leaving three vents on the top. When releasing the confining pressure used in gluing the faces together, the faces came apart on the right and bottom sides. These were reglued without applying confining pressure; thus the aperture toward the right and bottom is likely to be generally larger than at the top and left. All phenomena observed in the glass fracture models were observed in this experiment, including film flow, continuous rivulet flow, intermittent rivulet flow, REEs, drops falling rapidly through the fracture, and the development of a heat pipe. As in other experiments, finger and film length also decreased with increasing temperature. The falling drops occurred on the right side where the aperture was greater, with drops forming near the top of the replica, presumably at a location of contact or small aperture.

A feature referred to as a microfracture intersected the plane of the warmed region at an angle. Downward flow in the location of the microfracture was altered if the flow was slow. Rapidly moving drops passed the microfracture with their course unaltered. On the left side, where the aperture was narrower, a cell of boiling pentane existed in the warmed region, fed by pentane flowing down the microfracture and by a continuously and later intermittently flowing finger from a saturated island above the cell. This boiling cell was present at bath temperatures well above the pentane boiling point. The thermal conductivity of epoxy is much less than that of glass (~0.2 W $m^{-1}$ $K^{-1}$ versus ~1 W $m^{-1}$ $K^{-1}$), reducing heat transfer from the bath to the fracture aperture, perhaps more accurately modeling heat transfer in large fractured rock masses.

Experiment 16 was conducted to visualize liquid flow under vaporizing conditions in a natural fracture geometry with one real rock face. The fracture model was assembled from an epoxy replica of one fracture face and the corresponding rock face from a natural Topopah Spring tuff fracture from a specimen obtained from Fran Ridge, Nevada. In the manufacture of the silicone mold from which the epoxy replica was made, water was used to saturate the rock instead of using a mold release in an attempt to provide a more accurate impression of surface roughness and to leave the rock surface topography and chemistry as pristine as possible. Saturation was not complete, however, and some silicone imbibed into the rock, altering the rock's wettability from initially very water wetting to water repelling. This rock face was not used in the experiment. Visual inspection suggests that the surface of the epoxy replica made in the silicone mold has approximately the same roughness as the rock surface.

The dry rock was heated using heating tapes set at between 65° and 100°C for 6 hours and with a heat gun for 20 min, after

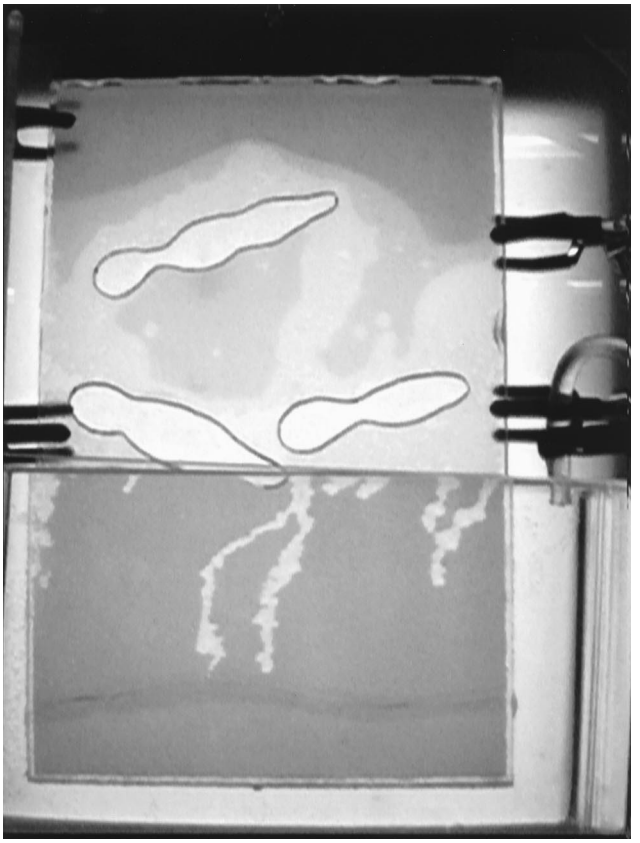

**Figure 8.** Longer fingers through model center: experiment 11, $T_{bath}$ = 37.1°C.

which temperature measurements indicated that a large area of the rock fracture face was above the pentane boiling point. The epoxy face was affixed to the warm rock and allowed to equilibrate for 8 min, after which the replica was removed and a thermal image of the rock surface was obtained. The epoxy face was replaced, and eight 1–3 mL volumes of pentane were introduced with two additional disassemblies to record thermal images of the rock surface. Because of evaporation and imbibition into the initially dry, hot, large rock (~130 kg), each addition of pentane was visible for ~1 min. Above the warmed region, pentane flowed in films, intermittent rivulets, and continuous rivulets into the warmed region. Films were visible on either or both fracture faces but when present on both, were narrower on the rock than the epoxy because imbibition. Once in the warmed region, pentane boiled rapidly, and fingers broadened. Flow persisted in fingers, but no films were seen. Pentane seeped more deeply into the warmed region when increased volumes of pentane were introduced and as the fracture cooled from its initial hot temperatures.

## 4. Heat Pipe Development

Thermal images obtained under roughly steady state conditions for experiments 9, 11–13, and 15 are presented in Plates 1–6. Prior to the introduction of pentane into the fractures, temperature gradients near the interface between the warmed and ambient regions are generally steep (Plate 4), characteristic of heat transfer from an extended surface. With pentane in the aperture and the bath temperature exceeding the boiling point, large regions of small temperature gradients have been observed, indicating the presence of convective heat transfer by vapor-liquid counterflow (heat pipes). This was verified in an experiment not presented here in which pentane containing a nonvolatile dye was introduced into a model. The dye was rapidly left at the edges of fingers in the warmed region rather than circulating in the condensation halo, indicating that liquid buoyant convection was not significant here. An example is shown in Plate 5.

The shape of the heat pipe region is strongly affected by the structure of the aperture. In the thermal image in Plate 5 the bright green protrusions on the left and right sides indicate heat pipe conditions in these locations. The video image (Plate 5 (right)) shows corresponding unsaturated conduits in these locations. Toward the center and adjacent to these unsaturated conduits are cooler saturated islands of pentane, indicated in the thermal image by the darker green. The central bright green region contains darker green spots that correspond to the locations of pentane islands saturating the aperture. In experiment 11, heat pipe development was strongly affected by the impermeable barriers (Plate 6). Pentane vapor was forced to travel vertically on the left and right sides of the model because of the impermeable barriers and the presence of liquid spanning the aperture in the center of the funnel structure. These warmed heat pipe regions are indicated by the brighter green color. In the center, temperatures are lower, indicating predominant downflow of cooled liquid. The most uniform heat pipe region was found in experiment 12 (Plate 1) where the aperture variability was minimal. Because of the wide aperture, pentane was present only in films on the fracture walls. The bright green region shows a very nearly constant temperature which was larger when more pentane was present in the model. The shape of the heat pipe region in experiment 13 was influenced by the presence of the large vent on the upper right side of the model (Plate 2). Newly vaporized pentane in this experiment was pushed toward the right boundary where the pressure was ambient, producing a bulge in the condensation halo and longer fingers on the right. In experiment 14 the aperture was very narrow which severely restricted liquid and vapor flow and limited heat pipe development. The temperature field resembled that shown in Plate 4. An uneven heat pipe (Plate 3) formed in the Stripa fracture replica (experiment 15) that was predominant on the right side where the aperture was wider, providing less viscous resistance to flow. No heat pipe was observed in rock/replica experiment, experiment 16, because insufficient liquid was present in the system to furnish the partial rock saturation needed to produce this phenomenon.

## 5. Discussion

Three types of liquid flow have been visually observed in the fracture models. These are described here as continuous rivulet flow, intermittent rivulet (and drop) flow, and film flow. In the laboratory experiments, continuous rivulet flow occurred during the initial rapid introduction of pentane into the models and replicas. In this flow the gravitational forces exceed the capillary and viscous forces, which would tend to stabilize islands of pentane in the fracture. The direction of flow responds to the gravitational, capillary, and viscous forces controlled by aperture heterogeneity. Continuous rivulet flow would occur in geologic media in locations where a constant supply of water was present, either because of infiltration or the confluence of smaller flows due to heterogeneities or impermeable barriers.

Intermittent rivulet flow occurs when there is only a slight

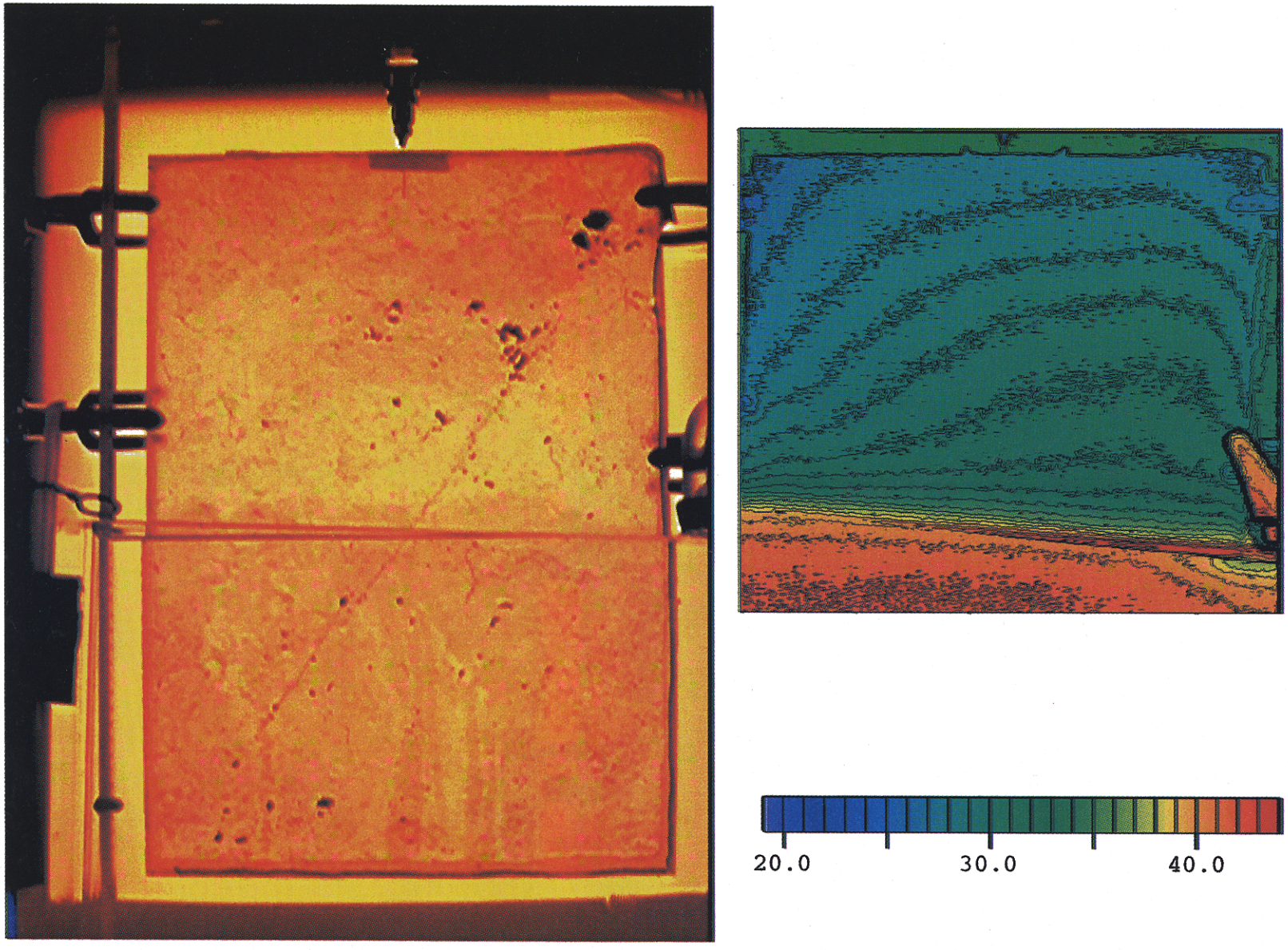


**Plate 3.** (left) Pentane and (right) temperature distributions: experiment 15, 42.2°C $< T_{\text{bath}} <$ 42.4°C. The thick, low conductivity epoxy makes the green heat pipe region more difficult to see. The heat pipe is more predominant on the right side where the aperture is larger.

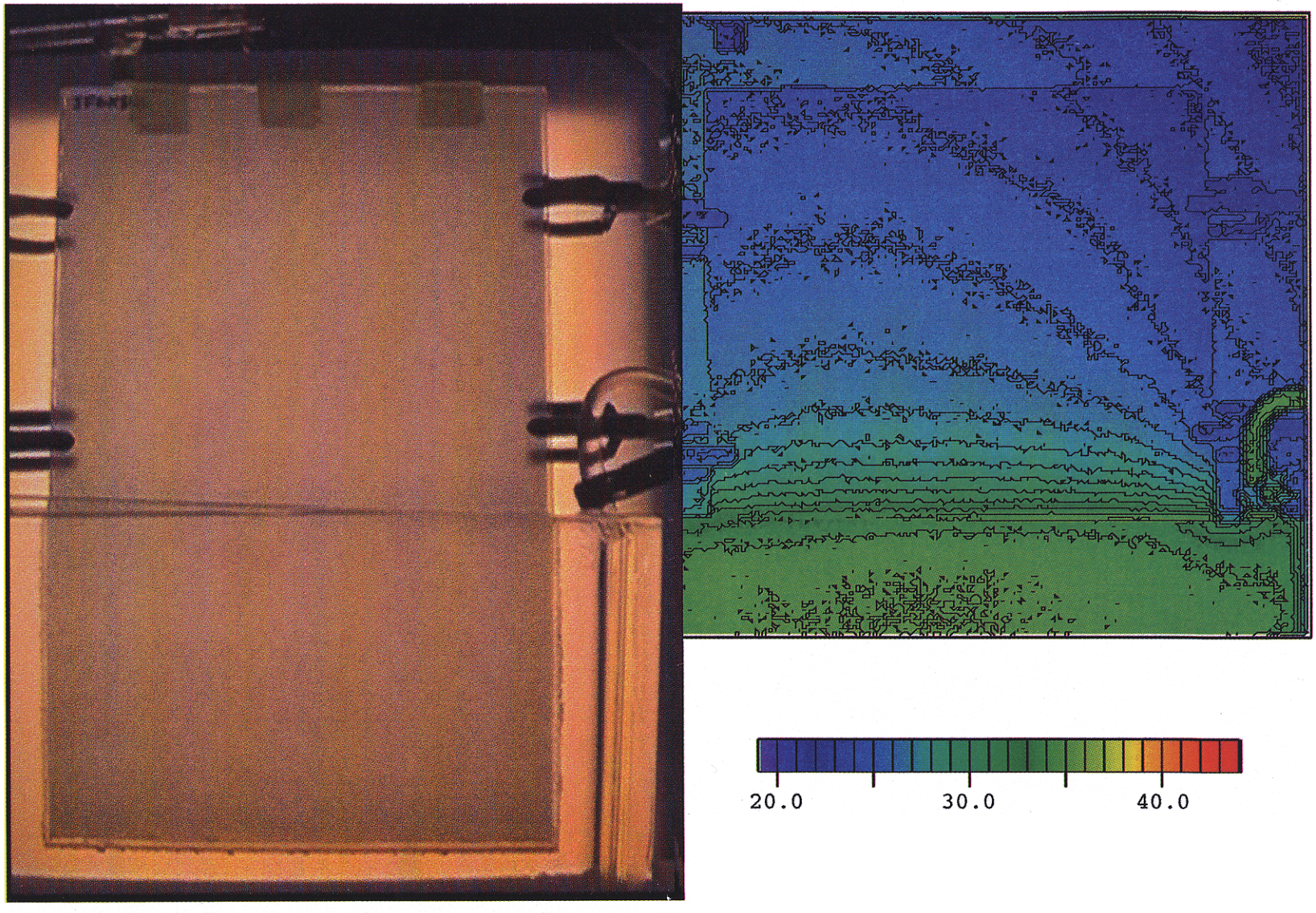


**Plate 4.** (left) Model without pentane (right) and initial temperature distribution: experiment 9, $T_{bath}$ = 36.4°C. Note steep temperature gradient near the interface between the warmed and cool region (top of water bath).

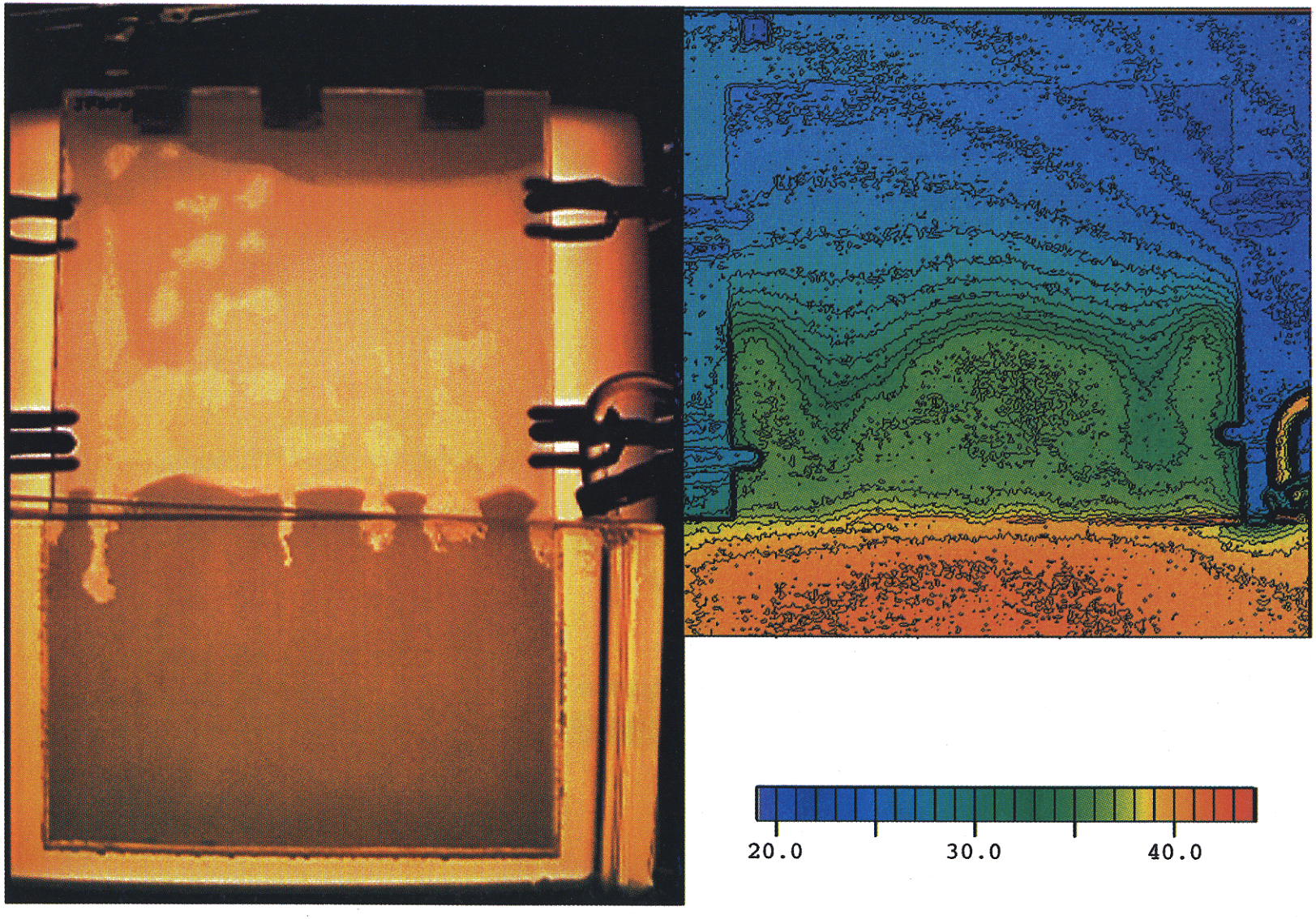


**Plate 5.** (left) Pentane and (right) temperature distribution: experiment 9, $T_{bath}$ = 42.4°C. The bright green region is near the boiling temperature and has a very small temperature gradient, characteristic of heat pipe conditions.

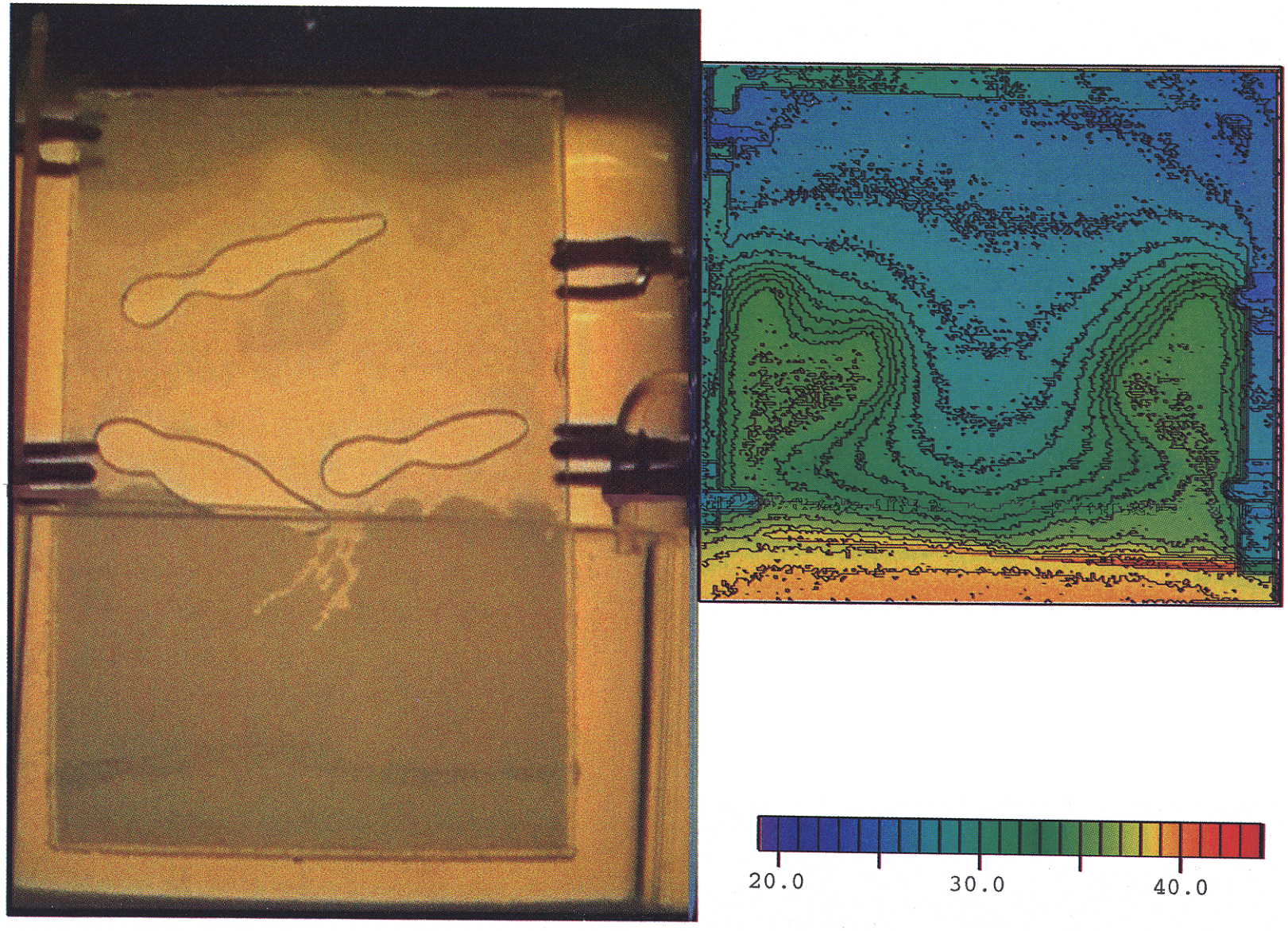


**Plate 6.** (left) Pentane and (right) temperature distributions: experiment 11, $T_{bath}$ = 41.3°C. Bright green heat pipe regions are on the left and right sides.

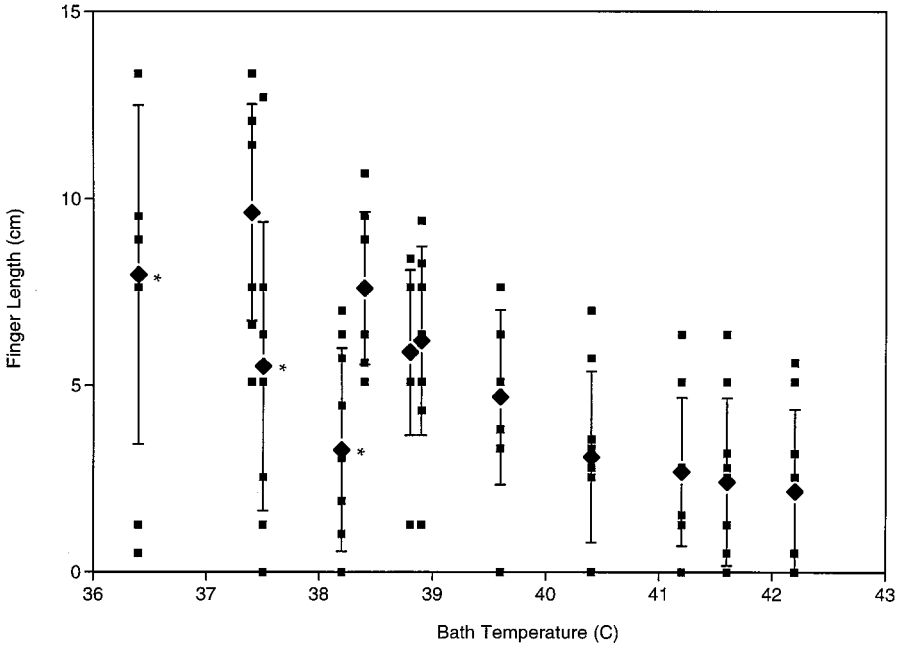


**Figure 9.** Finger length versus temperature. Squares represent individual finger lengths, and diamonds represent the average finger length at a given time. Asterisks identify finger lengths measured during cooling. Error bars represent 1 standard deviation.

imbalance between the stabilizing capillary forces and the destabilizing gravitational forces. These events occur when liquid is held in saturated islands, which are roughly in equilibrium with destabilizing forces. When additional fluid is added to these saturated islands either by flow or condensation, the destabilizing forces exceed the stabilizing capillary forces, and liquid from the saturated island flows in response to the imposed forces. This flowing liquid may contact other saturated islands and destabilize them, adding volume to the flow. It is expected that intermittent rivulet flow will occur in geologic media any time the rate of water seepage into a region exceeds the capacity for the water to flow onward via film flow but is less than the rate necessary to sustain continuous rivulet flow. Drop flow is an extreme example of intermittent rivulet flow. This occurs when liquid accumulates at a contact point above a wide vertical aperture. When a sufficient volume collects such that gravitational force exceeds the capillary force, a drop snaps off and falls. In wide vertical fractures, liquid may fall freely without contacting the fracture walls.

Film flow occurs when the aperture is large compared to the film thickness. Depending on suction pressures and surface topography, such films may be of the order of tens of microns thick [*Tokunaga and Wan*, 1997], much thicker than thin adsorbed water films which are of the order of tens to a hundred angstroms thick [*Gee et al*., 1990]. Thick films move on the fracture walls in response to gravitational forces and capillary forces imposed by the surface roughness. Film flow may be the slowest of the three observed flow types but may be the dominant flow mechanism transporting condensate to saturated islands and under low flow conditions. Films appeared unstable in some conditions, however. Film zones present where the fracture wall temperature exceeded the boiling temperature rapidly disappeared when intermittent rivulets flowed through. This may be due to the formation of saturated islands above the warmed region. Saturated islands may exist at a lower pressure because of capillarity than the thick films and induce film flow toward the islands. This reduces the amount of liquid flowing downward in films. Once the saturated islands are formed, liquid will collect there until the island becomes unstable and an intermittent rivulet is released. All of these conditions, continuous rivulet flow, intermittent rivulet flow, and film flow, are expected to occur when a strong heat source is placed into partially saturated fractured rock.

In all experiments, except experiment 12 in which only film and drop flow occurred, fingers penetrated some distance into the warmed region. In some experiments, films also penetrated into the warmed regions, primarily in wider aperture regions of fracture models. The depth of penetration of both films and fingers decreased with the increasing temperature of the water bath. The typical trend for average finger length and its variability are displayed in Figure 9 for experiment 9 (thick glass). A comparison of finger length measurements to theoretical analysis [*Phillips*, 1994, 1996] has not yet been performed.

While liquid was present in experiment 16, the phenomena which occurred were consistent with the phenomena which occurred in the other experiments, with the exception of imbibition which was only observed in this experiment. The imbibition served to reduce the observation time. Imbibition of liquid from repeated or constant introduction would tend to decrease as the saturation within the rock increased. Because the rock was initially totally unsaturated of pentane and contained a large quantity of heat compared to the small volumes of pentane added, the observations may be representative only of small flows in hot, very dry fractures such as intermittent flows very near a heat source. Because of this, the observations are not considered to be representative of all liquid flow in heated fractures where flow rates, water saturation, and relative humidity may be much greater. Better matching of liquid volumes to rock size and heat content will be attempted in future experiments.

The general conditions necessary for heat pipe formation include (1) a region at a temperature exceeding the liquid boiling point (evaporation zone), (2) adequate space and driving forces for vapor and liquid counterflow, and (3) a region cooler than the liquid boiling point (condensation zone). In all of these experiments the driving force for liquid return was gravity. Horizontal flow due to capillary forces was observed in some cases within the condensation halo, but the liquid was ultimately returned to the warm region by gravity. In one of the five experiments where heat pipes were observed (experiment 12), liquid return was in films; in the other four experiments, liquid return to the evaporation zone was primarily in fingers. Within the condensation halo (condensation zone), fingers and films were responsible for liquid flow.

In experiment 12 (Plate 1), good heat pipe conditions exist, and the condensation halo is uniform. The wide aperture provides for minimal interference between the liquid and vapor flow. In experiment 11 (Plate 6), gas flow is hindered by the impermeable barriers and liquid saturation in the model center. Similarly, the liquid flow through the funnel center was hindered by the increased pressure in the model bottom. Saturated islands, such as those in Plate 5, may act like impermeable barriers to the vapor transport, while at the same time the liquid may be flowing.

No heat pipe was observed in experiment 14, where the aperture was small, and liquid flow was controlled by viscous resistance. The rate at which pentane flowed into the warmed region, evaporated, and condensed was not large enough such that thermal images registered significant deviation from the original condition. The condition for adequate space for vapor-liquid counterflow was not met in this experiment.

## 6. Conclusions

Emplacement of heat-generating nuclear waste packages in a partially saturated fractured rock environment is expected to give rise to complex two-phase (liquid-gas) flow phenomena with phase change (boiling and condensation). Of particular interest are heat-driven flows in fractures, which could cause "fast" migration of water and solutes along localized preferential pathways. The objective of the current work is to obtain a better understanding of the relevant phenomena through laboratory-scale experimentation under controlled and monitored conditions.

We have studied thermally driven flows in a variety of laboratory fracture specimen using glass plates of different small- and large-scale surface roughness, an epoxy replica of a natural rock fracture, and an actual rock-replica fracture. The typical scale of the experiments was 20–30 cm. Pentane, with a boiling point of 36.1°C, was used as a volatile fluid instead of water to facilitate the experiments. Flow behavior was observed visually, and spatially resolved temperature monitoring was performed. Our initial experiments have demonstrated the following phenomena: boiling and condensation; formation of dry-out zones; flow funneling, focusing, and bypassing; localized preferential flow of liquid in nominally superheated regions; capillary-driven flow; and film flow. The presence of heat pipe processes (vapor-liquid counterflow) was inferred from observations of extended regions with very nearly isothermal conditions. Liquid flow in fingers and films in the heat pipes observed in these experiments was gravity-driven. Fingering flow in intermittent and continuous rivulets occurred in pathways where aperture heterogeneity induced gravitational instabilities.

Spatial and temporal averaging used in much of the current numerical modeling of these phenomena ignore liquid flow in preferential pathways. This type of flow was frequently observed in these experiments. In nuclear waste disposal, condensate flow in preferential paths may be beneficially away from the waste or detrimentally toward the waste and thus requires a better understanding. Liquid flow in films on fracture walls has not been well incorporated in mathematical modeling. In low flow conditions or in wide fractures this may be the major mechanism of liquid flow. Rapid evaporation events temporarily altered liquid flow paths. These alterations, in addition to the pressure pulses resulting from the REE, could negate the effect of a capillary barrier which would otherwise occur at the intersection of a fracture and a cavity containing waste. These REEs also require greater understanding. Further studies with closer integration of laboratory, field, and mathematical experiments would aid in gaining a better understanding these phenomena and applying this understanding appropriately.

Future work will attempt to explore flow in a broader variety of fracture specimen, with special emphasis on actual rock fractures from Yucca Mountain. Different flow geometries will be explored, including nonvertical fractures. An effort will be made to use water as the working fluid and to monitor chemical changes, such as mineral dissolution and precipitation, during hydrothermal flows. Quantitative analysis of fluid flow and heat transfer mechanisms will be made, and issues of scale-up to conditions at Yucca Mountain will be considered. Close integration will be sought with ongoing in situ heater experiments at Yucca Mountain and with mathematical modeling studies of thermohydrologic behavior.

**Acknowledgments.** This work was supported by the Director, Office of Civilian Radioactive Waste Management, U.S. Department of Energy, through the memorandum purchase order EA9013MC5X between TRW Environmental Safety Systems, Inc., and the Ernest Orlando Lawrence Berkeley National Laboratory under contract DE-AC03-76SF00098. Comments provided by J. Birkholzer and B. Freifeld at the Lawrence Berkeley National Laboratory and by M. Pantazidou, M. McGuinness, and an anonymous reviewer were greatly appreciated.

## References

Birkholzer, J. T., and Y. W. Tsang, Forecast of thermal-hydrological conditions and air injection test results of the single heater test at Yucca Mountain, *Rep. LBNL-39789 UC-814*, Lawrence Berkeley Natl. Lab., Berkeley, Calif., 1996.

Birkholzer, J. T., and Y. W. Tsang, Pretest analysis of the thermal-hydrological conditions of the ESF drift scale test, *Level 4 Milestone SP9322M4*, Lawrence Berkeley Natl. Lab., Berkeley, Calif., 1997.

Buscheck, T. A., and J. J. Nitao, The analysis of repository-heat-driven hydrothermal flow at Yucca Mountain, paper presented at Fourth Annual High Level Radioactive Waste Management International Conference, Am. Soc. of Civ. Eng./Am. Nucl. Soc., Las Vegas, Nev., 1993.

Buscheck, T. A., and J. J. Nitao, The impact of buoyant, gas-phase flow and heterogeneity on thermo-hydrological behavior at Yucca Mountain, paper presented at Fifth Annual High Level Radioactive Waste Management International Conference, Am. Soc. of Civ. Eng./Am. Nucl. Soc., Las Vegas, Nev., 1994.

Fitzgerald, S. D., C. T. Wang, and K. Pruess, Laboratory and theoretical studies of injection into horizontal fractures, paper presented at 18th New Zealand Geothermal Workshop, Geothermal Inst., Univ. of Auckland, 1996.

Flint, A., J. A. Hevesi, and L. E. Flint, Conceptual and numerical

model of infiltration for the Yucca Mountain area, Nevada, *U.S. Geol. Surv. Water Resour. Invest. Rep*., *MOL. 19970409.0087, GS9609083122211.003*, *223*, 1996.

Gee, M. L., T. W. Healy, and L. R. White, Hydrophobicity effects in the condensation of water films on quartz, *J. Colloid Interface Sci*., *140*, 450–465, 1990.

Geller, J. T., G. Su, and K. Pruess, Preliminary studies of water seepage through rough-walled fractures, *Rep. LBNL-38810 UC-403*, Lawrence Berkeley Natl. Lab., Berkeley, Calif., 1996.

Gentier, S., Morphologie et comportment hydromechanique d'une fracture naturelle dans un granite sous constrainte normale, Ph.D. thesis, Univ. D'Orleans, Orleans, France, 1986.

Glass, R. J., and M. J. Nicholl, Quantitative visualization of entrapped phase dissolution within a horizontal flowing fracture, *Geophys. Res. Lett*., *22*, 1413–1416, 1995.

Glass, R. J., and D. L. Norton, Wetted-region structure in horizontal unsaturated fractures: Water entry through the surrounding porous matrix, paper presented at Third Annual High Level Radioactive Waste Management International Conference, Am. Soc. of Civ. Eng./Am. Nucl. Soc., Las Vegas, Nev., 1992.

Ho, C. K., K. S. Makai, and R. J. Glass, Studies of non-isothermal flow in saturated and partially saturated porous media, paper presented at Fifth Annual High Level Radioactive Waste Management International Conference, Am. Soc. of Civ. Eng./Am. Nucl. Soc., Las Vegas, Nev., 1994.

Kung, K.-J. S., Preferential flow in a sandy vadose zone, 1, Field observation, *Geoderma*, *46*, 51–58, 1990a.

Kung, K.-J. S., Preferential flow in a sandy vadose zone, 2, Mechanism and implications, *Geoderma*, *46*, 59–71, 1990b.

Lide, D. R., *CRC Handbook of Chemistry and Physics*, CRC Press, Boca Raton, Fla., 1990.

McGuinness, M. J., Steady-solution selection and existence in geothermal heat pipes, II, The convective case, *Int. J. Heat Mass Transfer*, *39*, 259–274, 1996.

McGuinness, M. J., Steady-solution selection and existence in geothermal heat pipes, II, The conductive case, *Int. J. Heat Mass Transfer*, *40*, 311–321, 1997.

Nicholl, M. J., R. J. Glass, and H. A. Nguyen, Gravity-driven fingering in unsaturated fractures, paper presented at Third Annual High Level Radioactive Waste Management International Conference, Am. Soc. of Civ. Eng./Am. Nucl. Soc., Las Vegas, Nev., 1992.

Nicholl, M. J., R. J. Glass, and H. A. Nguyen, Small-scale behavior of single gravity-driven fingers in an initially dry fracture, paper presented at Fourth Annual High Level Radioactive Waste Management International Conference, Am. Soc. of Civ. Eng./Am. Nucl. Soc., Las Vegas, Nev., 1993a.

Nicholl, M. J., R. J. Glass, and H. A. Nguyen, Wetting front instability in an initially wet unsaturated fracture, paper presented at Fourth Annual High Level Radioactive Waste Management International Conference, Am. Soc. Civ. Eng./Am. Nucl. Soc., Las Vegas, Nev., 1993b.

Nitao, J. J., V-TOUGH, an enhanced version of the TOUGH code for the thermal and hydrologic simulation of large-scale problems in nuclear waste isolation, *Rep. UCID-21954*, Lawrence Livermore Natl. Lab., Livermore, Calif., 1989.

Nitao, J. J., T. A. Buscheck, and D. A. Chestnut, The implications of episodic nonequilibrium fracture-matrix flow on site suitability and total system performance, paper presented at Third Annual High Level Radioactive Waste Management International Conference, Am. Soc. of Civ. Eng./Am. Nucl. Soc., Las Vegas, Nev., 1992.

Persoff, P., and K. Pruess, Two-phase visualization and relative permeability measurement in natural rough-walled rock fractures, *Water Resour. Res*., *31*, 1175–1186, 1995.

Phillips, O. M., Liquid infiltration through the boiling point isotherms in a dessicating fractured rock matrix, paper presented at Fifth Annual High Level Radioactive Waste Management International Conference, *Am. Soc. of Civ. Eng./Am. Nucl. Soc*., Las Vegas, Nev., 1994.

Phillips, O. M., Infiltration of a liquid finger down a fracture into superheated rock, *Water Resour. Res*., *32*, 1665–1670, 1996.

Pruess, K., On vaporizing water flow in hot sub-vertical rock fractures, *Transp. Porous Media*, *28*, 335–372, 1997.

Pruess, K., and Y. Tsang, Modeling of strongly heat-driven flow processes at a potential high-level nuclear waste repository at Yucca Mountain, Nevada, *Rep. LBL-33597 UC-200*, Lawrence Berkeley Natl. Lab., Berkeley, Calif., 1993.

Pruess, K., and Y. Tsang, Thermal modeling for a potential high-level nuclear waste repository at Yucca Mountain, Nevada, *LBL-35381 UC-600*, Lawrence Berkeley Natl. Lab., Berkeley, Calif., 1994.

Pruess, K., Y. W. Tsang, and J. S. Y. Wang, Numerical studies of fluid and heat flow near high-level nuclear waste packages emplaced in partially saturated fractured tuff, *LBL-18552*, Lawrence Berkeley Natl. Lab., Berkeley, Calif., 1984.

Pruess, K., J. S. Y. Wang, and Y. W. Tsang, Modeling of strongly heat driven flow in partially saturated fractured porous media, *Memoires*, *XVII*, 486–497, 1985.

Pruess, K., J. S. W. Wang, and Y. W. Tsang, Effective continuum approximation for modeling fluid and heat flow and heat flow in fractured porous tuff, *SAND86-7000*, Sandia Natl. Lab., Albuquerque, N. M., 1988.

Pruess, K., J. S. Y. Wang, and Y. W. Tsang, On thermohydrologic conditions near high-level nuclear wastes emplaced in partially saturated fractured tuff, 1, Simulation studies with explicit consideration of fracture effects, *Water Resour. Res*., *26*, 1235–1248, 1990a.

Pruess, K., J. S. Y. Wang, and Y. W. Tsang, On thermohydrologic conditions near high-level nuclear wastes emplaced in partially saturated fractured tuff, 2, Effective continuum approximation, *Water Resour. Res*., *26*, 1249–1261, 1990b.

Ramesh, P. S., and K. E. Torrance, Stability of boiling in porous media, *Int. J. Heat Mass Transfer*, *33*, 1895–1908, 1990.

Rossini, F. D., B. J. Mair, and A. J. Streiff, *Hydrocarbons From Petroleum, The Fractionation, Analysis, Isolation, Purification, and Properties of Petroleum Hydrocarbons*, Reinhold, N. Y., 1953.

Stubos, A. K., C. Satik, and Y. C. Yortsos, Effects of capillary heterogeneity on vapor-liquid counterflow in porous media, *Int. J. Heat Mass Transfer*, *36*, 967–976, 1993.

Su, G., Water infiltration and intermittent flow in rough-walled fractures, M.S. thesis, Univ. of Calif., Berkeley, 1995.

Tokunaga, T. K., and J. Wan, Water film flow along fracture surfaces of porous rock, *Water Resour. Res*., *33*, 1287–1295, 1997.

Tsang, Y. W., and K. Pruess, A study of thermally induced convection near a high-level nuclear waste repository in partially saturated fractured tuff, *Water Resour. Res*., *23*, 1958–1966, 1987.

Tsang, Y. W., and K. Pruess, Preliminary studies of gas phase flow effects and moisture migration at Yucca Mountain, Nevada, *Rep. LBL-28819*, Lawrence Berkeley Natl. Lab., Berkeley, Calif., 1989.

Udell, K. S., Heat transfer in porous media considering phase change and capillarity: The heat pipe effect, *Int. J. Heat Mass Transfer*, *28*, 485–495, 1985.

Vargaftik, N. B., *Tables on the Thermophysical Properties of Liquids and Gases*, John Wiley, New York, 1975.

Wark, K., *Thermodynamics*, McGraw-Hill, New York, 1977.

T. J. Kneafsey and K. Pruess, Earth Sciences Division, Lawrence Berkeley National Laboratory, University of California, Berkeley, CA 94720. (e-mail: tjkneafsey@lbl.gov)

(Received December 9, 1997; revised June 1, 1998;
accepted June 15, 1998.)